

UNIVERSITY OF CALIFORNIA
Santa Barbara

Pattern Formation in Binary–Fluid Mixtures
in Cylindrical Geometry

A Dissertation submitted in partial satisfaction
of the requirements for the degree of

Doctor of Philosophy

in the subject of

Physics

by

Kristina Lerman

August, 1995

Committee in charge:

Professor Guenter Ahlers

Professor David S. Cannell

Professor Jean Carlson

Copyright by
Kristina Lerman
1995

ACKNOWLEDGEMENTS

When people asked me about my plans for the future, as they did with increasing frequency over the past year or two, I told them I was in no hurry to graduate. What more could I ask for than the triple fortune of being young, living in a beautiful place, and working on a pretty problem with some of the best people in the field? It is not without some regret, but also with a sense of accomplishment that I close this chapter of my life. My six years at UCSB have been an enriching experience, and I would like to thank some people who have contributed to my formal and informal education.

I was lucky to have had two advisors, Guenter Ahlers and David Cannell, who wonderfully complemented each other. David's exacting standards for intellectual and scientific rigor, were a good training in clear and precise thinking. His advice has been a life saver at times when I got stuck on a particularly frustrating problem. Guenter's gift of physical insight trained me in the art of recognizing the important aspects of the physical problem and how to study them. I want to thank both for offering me guidance and support over the years.

My advisors helped create a great working and learning environment in the lab, an environment that a growing family of students and postdocs helped to maintain. I consider myself extremely fortunate to have worked in this group. I would like to acknowledge some of the people I worked with, who have added so much to my intellectual development, and helped me with my work: Eberhard Bodenschatz, Lipiin Sung, Lori Goldner, Melora Larson, Ning Li, Yuchou Hu, Ken Babcock, Feng-Chuan Liu, and Mike Dennin. I want to specially mention Stephen Morris, whose unorthodox way of thinking has enlivened many group meetings and dinner conversations. I am grateful to Art Bailey for his bottomless patience and willingness to help with the intricate hardware problems, of which there were many when I was starting out. I am most indebted to Steve Trainoff, who will always be an invaluable

resource for any group in which he finds himself. Most of the computer code I used in my work is some derivative of Steve's code. I learned a lot from Steve, both by asking for his help in solving problems, and by engaging him in conversations on all imaginable topics (everyone of which Steve had an opinion on). I will miss the countless hours spent in the computer room discussing all sorts of questions large and small.

I have learned much from the UCSB physics faculty, both in the classroom and in informal discussions, for which I would like to thank Jean Carlson in particular. I also want to thank my graduate school cohorts, the people to whom I gravitated intellectually, and with whom I shared many a conversation, a movie or a play, and a brisk enjoyment of nature. These include Ben Lee, Andrea Markelz, Shirley Pepke, Sean Quinlan, Laura Smilowitz and Lorene Samoska. These people added tremendously to my experience in Santa Barbara.

I could not have weathered all the frustrations of graduate school without the emotional support of the person closest to me. With warmest gratitude I thank Richard Ross, for his unflagging confidence in my ability, that has been a bridge for me to cross during periods of doubt. I also want to thank Richard for all the soul-rejuvenating experiences we had together, including beauties of nature and wonders of art.

I want to acknowledge my family, my grandmother Lyubov Slutskaya, and my mother Dolores Lerman who had the courage and strength to make the journey to this country some sixteen years ago from the former Soviet Union, which opened for me the opportunities I never would have had in that country. And I want to mention my brother Nathan, who has (mostly) been a joy, and who has, more significantly, taught me to boil water. As everyone knows, my work would have been impossible without this precious skill.

VITA

Born: March 1, 1967 in Kiev, former U.S.S.R.

- 1989 A. B., Princeton University.
1986–89 Research Assistant, Department of Physics, Princeton University.
1990–95 Graduate Student Researcher, Department of Physics,
 University of California, Santa Barbara.

PUBLICATIONS

1. *Different Convection Dynamics in Mixtures With the Same Separation Ration* K. Lerman, D. S. Cannell and Guenter Ahlers, *in preparation*.
2. *Study of Linear in Binary–Fluid Mixtures in Cylindrical Geometry* K. Lerman, D. S. Cannell and Guenter Ahlers, *in preparation*.
3. *Localized States in 2d Binary Liquid Convection* K. Lerman, E. Bodenschatz, D. S. Cannell and Guenter Ahlers, *Physical Review Letters*, **70**, 3572 (1993).
4. *Experiments in three systems with non variational aspects* E. Bodenschatz, D. S. Cannell, J. R. de Bruyn, R. Ecke, Y. C. Hu, K. Lerman and G. Ahlers, *Physica*, **D61**, 77 (1992).
5. *Spin relaxation due to magnetic field inhomogeneities: Quartic dependence and diffusion-constant measurements* K. C. Hasson, G. D. Gates, K. Lerman, P. Bogorad and W. Happer, *Physical Review A*, **41**, 3672 (1990).

ABSTRACT

An extensive study of convection in ethanol–water mixtures heated from below in cylindrical geometry is presented. Two mixtures, with 25.0–wt.% and 1.1–wt.% ethanol concentrations are studied. These mixtures have nearly identical negative separation ratios and exhibit a subcritical bifurcation to traveling waves. During the linear regime, while the radially traveling wave amplitude is small, convection patterns can be decomposed into independent azimuthal modes. The symmetry of the pattern depends strongly on the radial aspect ratio of the cell, $\Gamma \equiv R/d$. In both mixtures, even azimuthal modes are preferred for $\Gamma = 11.53$ and $\Gamma = 11.44$, while for $\Gamma = 10.91$, odd modes dominate. Demodulation of the time series of each mode’s amplitude is used to extract the spatial and temporal profiles of the in- and out-going waves. Solutions of the Ginzburg–Landau type equation describing propagating waves are fit to these profiles and the growth rates of the strongest modes are extracted. I measure the control parameter dependence of the growth rates and compare results for the three aspect ratios.

Evolution of the linear transient leads to a pattern in which convection amplitude is strongly enhanced along a diameter of the cell and weak elsewhere. In the 25–wt.% mixture, this transient usually lead to the formation of a long-lived localized pulse of traveling wave convection. This pulse persisted for a long time, but unlike 1d pulse, it was not ultimately stable. Depending on parameters, the pulse lost stability either by decaying to zero amplitude or by becoming disordered and spreading so as to fill the cell. In the 25.0–wt.% mixture, the cell always filled with convection rolls when the control parameter was above its threshold value. Dynamics of convection patterns is drastically different in the 1.1–wt.% mixture for similar experimental parameters. For a range of supercritical control parameter, irregularly repeated transients and aperiodically fluctuating regions of disordered convection that persist for days are observed.

Contents

1	Introduction	1
1.1	Pattern formation — the Big picture	1
1.2	Fundamentals of thermal convection in binary fluid mixtures	7
1.3	Theoretical Background	12
1.3.1	Equations of motion of a two component fluid	13
1.3.2	Linear stability analysis	14
1.4	Amplitude equation	15
1.5	Experiments on binary–fluid convection	23
1.5.1	Linear transients of TW convection	23
1.5.2	Localized pulses of convection	28
1.5.3	Spatio–temporal complexity	33
2	Experimental Set-up	36
2.1	Cell Design	36
2.1.1	Top Plate	38
2.1.2	Bottom Plate	39
2.1.3	Sidewalls	40
2.1.4	Cell Assembly	41
2.1.5	Mixture Preparation	42
2.2	Temperature Regulation	43
2.3	Shadowgraph	44
2.4	Image division	49

3	Linear Transients	51
3.1	Symmetry of patterns at onset	52
3.2	Mathematical description of linear transients	53
3.3	Analysis of linear transients: Separation of modes	57
3.3.1	Finding the center of the cell	58
3.3.2	Cosine transform of the image	58
3.3.3	Time series analysis	60
3.3.4	Temporal and spatial profiles of right TW	64
3.3.5	Reflection Coefficient	67
3.4	Convection in 25% ethanol–water mixtures in two different geometries	68
3.4.1	Linear transients in the $\Gamma = 10.91$ cell	68
3.4.2	Linear transients in the $\Gamma = 11.53$ cell	77
3.5	Linear transients in a 1.1% ethanol mixture	83
4	Nonlinear Transients	92
4.1	Azimuthal focusing	93
4.2	Localized pulses in 25–wt.% ethanol–water mixtures.	101
4.3	Repeated transients in 1.1–wt.% alcohol mixture	111
4.4	Constant heat flux experiments in high ethanol concentration mixtures	120
	Conclusion	126
	Appendices	129
A	Fluid parameters	129
	C program	132
B	Fitting the image	147
B.1	Wave equation in cylindrical geometry	148
B.1.1	Hankel functions	148

B.1.2	Spatial growth	148
B.1.3	Procedure for fitting images	149
B.2	Compressible Fluid Flow — Damping	152
B.2.1	Procedure for fitting images	153
B.2.2	Discussion of the results	155
B.2.3	$\Gamma = 11.53$ cell	155
B.3	Example of an image-fitting C program	157
C	Supplementary information	163
	References	167

List of Figures

1.1	Schematic of a convecting fluid layer.	9
1.2	Separation ratio vs. concentration of alcohol in ethanol–water mixtures	11
1.3	Critical Rayleigh number <i>vs</i> ψ for binary–fluid mixtures . . .	16
1.4	Localized pulse of TW convection in rectangular cell	28
2.1	Schematic of the apparatus	37
2.2	Detailed schematic of the convection cell	38
2.3	Temperature of the bath measured by bottom plate thermistor over 21 hours.	44
2.4	Shadowgraph	47
2.5	Diagram of the combined lens-convection roll optical system. .	48
3.1	Azimuthal modes at the onset of convection in $\Gamma = 10.91$ and $\Gamma = 11.53$ cells	54
3.2	Horizontal scan across divided image of the conduction state .	59
3.3	Analysis of $m = 1$ mode	61
3.4	Time series of $m = 1$ mode, right TW, and their envelope . . .	63
3.5	Fourier transform space and filter that keeps the region corresponding to right TW	64
3.6	Line scans showing the temporal and spatial evolution of the envelope of right TW	66
3.7	Azimuthally averaged amplitude $\sqrt{r}A_m$ for even modes in the $\Gamma = 10.91$ cell	69
3.8	Time series of $m = 3$ mode, right TW, and their envelope in the $\Gamma = 10.91$ cell	70
3.9	Temporal and spatial profiles of the envelope of right TW of the $m = 1$ and $m = 3$ modes	72
3.10	Analysis of $m = 3$ mode	73

3.11	Time series of odd modes, and the envelope of right TW from the run in which $m = 3$ mode is dominant	74
3.12	Temporal and spatial profiles of the envelope of right TW for the strongest odd modes in a $\Gamma = 10.91$ cell	75
3.13	Spatial and temporal growth rates versus ϵ in the $\Gamma = 10.91$ aspect ratio cell	76
3.14	Analysis of azimuthal modes in a cell that selects even modes	78
3.15	Time series of the $m = 0$ mode in the $\Gamma = 11.53$ cell	79
3.16	Time series of the even modes in the $\Gamma = 11.53$ cell	80
3.17	Temporal and spatial profiles of the envelope of the right traveling waves of the first four azimuthal modes in the $\Gamma = 11.53$ cell	81
3.18	Spatial and temporal growth rates versus ϵ in a $\Gamma = 11.53$ aspect ratio cell	83
3.19	Analysis of azimuthal modes in the $\Gamma = 11.44$ cell with a low alcohol concentration mixture	85
3.20	Analysis of azimuthal modes in a cell that selects even modes	86
3.21	Timeseries of the $m = 0$ mode, right TW, and their envelope .	87
3.22	Temporal and spatial profiles of the envelope of the right traveling waves of the first five azimuthal modes in a $\Gamma = 11.44$ cell	88
3.23	Spatial and temporal growth rates versus ϵ in a $\Gamma = 11.44$ aspect ratio cell with a 1.1% alcohol mixture	89
4.1	Nonlinear transients and localized pulse	94
4.2	Nonlinear transients in the $\Gamma = 10.91$ cell, 25% alcohol mixture	96
4.3	Amplitudes of outgoing waves vs time in the $\Gamma = 10.91$ cell . .	97
4.4	Dimensionless angular frequencies of traveling waves during linear and nonlinear transients for $\Gamma = 10.91$ and $\Gamma = 11.53$. .	98
4.5	Azimuthally focusing nonlinear transients for $\Gamma = 10.91$ and 25% by weight alcohol mixture	99
4.6	Outgoing wave amplitudes of different azimuthal modes in the $\Gamma = 10.91$ cell	100
4.7	Image of a cell filled with stationary overturning convection rolls	100
4.8	Azimuthally focusing nonlinear transients in the $\Gamma = 11.44$ cell with a 1.1% alcohol mixture	102
4.9	Outgoing wave amplitudes of different azimuthal modes in the $\Gamma = 11.44$ cell with a 1.1% alcohol mixture	103
4.10	Localized pulses in 1d and 2d geometries	103

4.11	Nusselt number plot for 25–wt.% alcohol mixtures in the $\Gamma = 11.53$ cell	104
4.12	Nonlinear states and the “hole” in the $\Gamma = 11.53$ cell with a 25% alcohol mixture	106
4.13	Images taken in the $\Gamma = 11.53$ cell, with a 25% alcohol mixture, showing the formation of a “hole”	107
4.14	Time series of the Nusselt number for two runs in which a “hole” is formed, and for a long–lived localized pulse	108
4.15	Localized pulse of convection in a $\Gamma = 11.53$ cell	109
4.16	Defect propagation in the pulse	110
4.17	Nusselt number vs ϵ for 1.1% alcohol negative separation ratio mixture in a $\Gamma = 11.44$ cell	112
4.18	“Wall” state in a 1.1% alcohol mixture	112
4.19	Time series of the Nusselt number for two runs in the 25% and 1.1% alcohol concentration mixtures	113
4.20	Images from the repeating transient regime at in the 1.1–wt.% alcohol mixture	114
4.21	Nusselt numbers recorded during erratic transients in the 1.1% ethanol–water binary fluid	116
4.22	Histogram of Nusselt numbers recorded during erratic transients in the 1.1% ethanol–water binary fluid.	117
4.23	Convection patterns recorded during erratic transients in the 1.1% ethanol–water binary fluid	118
4.24	Images during a constant heat flux run in the $\Gamma = 11.62$ cell with a 25% alcohol mixture	122
4.25	Nusselt number time series during the constant heat flux experiment with a 25% alcohol mixture	123
4.26	A “triangle” and a “zipper” in a 25% mixture	125
B.1	Raw images and patterns generated using results of fits: exponential spatial growth rates.	151
B.2	Results of fitting a sequence of images to cylindrical traveling waves with an exponential spatial growth rate.	152
B.3	Results of fitting solutions of cylindrical traveling waves in a medium with gain to images in a $\Gamma = 10.91$ cell.	154
B.4	Results of fitting a sequence of images to cylindrical traveling waves in a medium with gain.	156
B.5	Raw images in a $\Gamma = 11.53$ cell and patterns generated using results of fits to the raw patterns.	156

List of Tables

1.1	Analogies between phase transitions in equilibrium systems and pattern formation in nonequilibrium systems.	5
3.1	Linear regression of the temporal and spatial growth rates of azimuthal modes	90
3.2	Reflection coefficient and threshold shift	91
A.1	Experimental parameters describing the mixtures	131
A.2	Physical mixture parameters	131
A.3	Theoretical parameters describing the mixtures	131
A.4	Calculated mixture parameters	132
B.1	$\Gamma = 10.91$ cell : Results of fits of convection patterns to solutions of the form Eqn. B.6.	151
B.2	$\Gamma = 10.91$ cell : Results of fits of convection patterns to solutions of the form Eqn. B.9.	154
C.1	Spatial and temporal growth rates of the $m = 1$ mode versus ϵ in a $\Gamma = 10.91$ aspect ratio cell.	163
C.2	Spatial and temporal growth rates of the $m = 3$ mode versus ϵ in a $\Gamma = 10.91$ aspect ratio cell.	164
C.3	Spatial and temporal growth rates of the $m = 0$ mode versus ϵ in a $\Gamma = 11.53$ aspect ratio cell.	164
C.4	Spatial and temporal growth rates of the $m = 2$ mode versus ϵ in a $\Gamma = 11.53$ aspect ratio cell.	165
C.5	Spatial and temporal growth rates of the $m = 4$ mode versus ϵ in a $\Gamma = 11.53$ aspect ratio cell.	165
C.6	Temporal growth rates of the $m = 1$ mode versus ϵ in a $\Gamma = 11.53$ aspect ratio cell.	166

Chapter 1

Introduction

1.1 Pattern formation — the Big picture

Even the most casual glance at the world reveals that there is much order and structure in nature. Regular structures, patterns, often arise spontaneously in otherwise uniform systems, usually in response to some external stress. For centuries humankind has been fascinated with the natural patterns they saw around them — orderly rows of clouds and ocean waves extending for miles, the washboard pattern of sand ripples on river bottoms and in deserts, and countless examples of patterns in biological systems, from the ordered growth of some bacterial colonies to the skin colorations of animals. It would not be too surprising to learn if the physical mechanisms of pattern formation will be shown to have been coopted by evolution to assist in cell differentiation and organism development.

Physical mechanisms of pattern formation

Patterns often arise in dissipative systems that are far from equilibrium in response to some external stress. For this reason they are often called dissipative structures. Thermal convection in a fluid heated from below (also

known as Rayleigh-Bénard convection) is one of the physicists' favorite pattern forming systems, because it enables one to create orderly nontrivial structures under highly controlled conditions, and because the microscopic physics governing the behavior of the system is well understood. The hydrodynamic equations of fluid motion are presented in Sec. 1.3.1. Rayleigh-Bénard convection results from the competition between the driving buoyancy force, that is the warmer fluid's tendency to rise, and the equilibrating effects of thermal conduction and viscous dissipation. As the stress parameter is increased beyond some critical value (in the case of Rayleigh-Bénard convection the stress parameter is the temperature difference applied across the fluid layer), the buoyancy forces overcome dissipation, and the system becomes unstable to the formation of a pattern. Another intensively studied system is Taylor-Couette flow, which is the flow of a fluid confined between concentric rotating cylinders[1, 2]. Some newer experimental systems include thermal[3] and electrohydrodynamic[4] convection in nematic liquid crystals, Faraday surface waves that result from a parametric oscillation of horizontal layer of fluid[5], and spatial patterns in chemically reacting systems[6]. This list of inanimate pattern forming systems is by no means exhaustive. Interest in biological patterns has also been growing. It has been noted that some phototropic algae form beautiful hexagonal arrays. The instability mechanism responsible for these structures is the competition between algae's tendency to swim upwards to the water surface where oxygen and sunlight are plentiful and its tendency to sink, since it is heavier than the surrounding fluid.

Amplitude equation formalism of pattern formation

Patterns can arise in systems governed by very different microscopic physical laws. However, many of these different pattern forming systems share common features. These features include existence of a well defined onset, that is the point at which the uniform base state loses stability to a state with a pattern, selection of a preferred wave vector at onset, and system's response

to the forcing parameter. The many similarities exhibited by diverse systems suggest that the theory of pattern formation should be general, therefore, system independent. The amplitude equation formalism is one successful and widely used approach that is used in the study of pattern formation in systems with different underlying physical mechanisms. This theory studies the dynamics of the amplitude of the pattern, e.g. strength of convective flow, close to the threshold of pattern formation. The details of the microscopic physics do not determine the structure of the amplitude equation; they appear only through the parameters of the theory. Coarse grained theories, where explanation of the system at one level is independent of the explanation on a more fundamental level, are familiar to physicists. Coarse-graining is prevalent in fluid mechanics. At the most fundamental level of description, the fluid is a collection of interacting molecules. However, the fundamental unit in hydrodynamics, the next level of description, is the hypothetical fluid “bubble.” Molecular physics formalism contributes the physical fluid parameters, such as viscosity and diffusivity, to the hydrodynamic description. The details of the hydrodynamics framework are in turn irrelevant to the amplitude equation formalism, the next level of explanation, and contribute to it only through a set of dimensionless parameters that specify the system.

Amplitude equation formalism is the unifying theory of pattern formation close to threshold, because it can be applied to a number of systems with different instability mechanisms. Thus, the same amplitude equation, albeit with different coefficients, describes thermal convection in binary–fluid mixtures, electro-hydrodynamic convection of nematic liquid crystals, and the Taylor-Couette system with throughflow. In the following sections I will look more closely at the amplitude equations that describe such systems.

Analogy with phase transitions

Pattern formation in nonequilibrium systems has many analogs in phase transitions in equilibrium systems, though the reason for this extensive analogy

has eluded physicists. Just as in equilibrium physics a uniform system can break its spatial (or some other) symmetry when the control parameter (for instance the temperature) passes some threshold value, pattern forming systems break spatial and sometimes time symmetry when the control parameter passes its critical value. In an equilibrium ferromagnetic system, the control parameter measures distance along the temperature axis from threshold, the Curie temperature. In Rayleigh-Bénard convection, for instance, the control parameter is the distance away from the critical temperature difference required to start convection. When this threshold is crossed in equilibrium systems, an order parameter, defined to be zero “below” the phase transition and non-zero “above”, begins to grow. A second order phase transition in equilibrium systems occurs when the order parameter grows continuously from zero as the transition is crossed. In pattern forming systems, a continuously increasing amplitude defines a forward bifurcation. A first order phase transition, and its analog the backward bifurcation, are defined to occur when the order parameter, or the amplitude, is discontinuous at the threshold value of the control parameter. Some examples of equilibrium phase transitions include growth of crystal structure in solidification, appearance of magnetic order in ferromagnets, the superfluid transition in liquid helium. Examples of pattern forming systems are far too numerous to exhaustively enumerate. The systems studied in our laboratory include thermal convection in liquids[7], gases[8, 9, 10, 11] and fluid mixtures[12], in which roll, square and hexagonal patterns have been observed, Taylor-Couette flow between rotating concentric cylinders[13, 14], and thermal[3] and electrohydrodynamic[4] convection in nematic liquid crystals in which a variety of patterns and temporal behaviors has been observed. The similarities and differences between equilibrium phase transitions and nonequilibrium pattern formation are summarized in table 1.1.

Table 1.1: Analogies between phase transitions in equilibrium systems and pattern formation in nonequilibrium systems.

	Phase Transitions	Pattern Formation
system	equilibrium	non-equilibrium
control parameter macroscopic quantity	$\epsilon = T/T_c - 1$	$\epsilon = \Delta T/\Delta T_c - 1$ $\epsilon = V^2/V_c^2 - 1$
	order parameter = 0 for $\epsilon < 0$ $\neq 0$ for $\epsilon > 0$	amplitude = 0 for $\epsilon < 0$ $\neq 0$ for $\epsilon > 0$
continuous transition discontinuous transition	second order first order	forward bifurcation backward bifurcation
examples	magnetic order crystal structure etc.	thermal convection (rolls, squares, hexagons) EHC in nematics etc.
		Hopf bifurcation localized states spatio-temporal chaos turbulence

Binary–fluid convection as a paradigm for the study of dynamical systems

Nonequilibrium systems also exhibit phenomena that are absent in phase transitions, but ubiquitous in the real world. These phenomena include Hopf bifurcations (that is transitions to a time–periodic state), localized pulses in which one phase coexists with another phase over a range of the control parameter, and spatio-temporal complexity which at very high values of the control parameter takes the form of turbulence. Convection in binary–fluid mixtures demonstrates all three of the above behaviors. Moreover, these phenomena are usually observed close to the convection threshold, raising the possibility of a theoretical description. Indeed, because the fundamental laws describing convection in binary–fluid mixtures are well understood,

the system is an attractive paradigm for the study of dynamical systems. Convection in binary–fluid mixtures has been studied extensively in narrow cells, either rectangles or annuli, that are one-dimensional manifestations of three-dimensional convective flow. Simplification of the underlying theory that results from the reduced dimensionality, has led to progress in theoretical understanding of the system along the analytical and numeric fronts. How what is understood about one-dimensional systems can be applied to convection in wide cells, and what complications in dynamics the extra degree of spatial freedom introduces, is the focus of my experiments. While theory and experiment in the field have progressed hand in hand over the past decade, the extreme complexity of the two dimensional systems puts us at the limit of the current power of theoretical investigations. At the same time, in order to make progress in understanding pattern formation in the real world, we need to master the more realistic model of it, namely convection in wide cells. I hope that my experiments might prove a useful guide to future investigators who might endeavor to shed some light on the observed phenomena.

Overview

The sections below discuss some of the aspects of the theoretical understanding of this system. I present the hydrodynamic equations of motion of binary–fluid mixtures, describe the linear stability analysis and the amplitude equations. In the concluding sections of this chapter, I highlight some experimental results, stressing the connection between theory and experiment, particularly from the point of view of amplitude equations. Chapter 2 describes the care taken to construct a uniform system, with as small an inhomogeneity in the control parameters as possible. Chapter 3 discusses how taking advantage of azimuthal symmetry of the cylindrical convection cell, allows me, in effect, to reduce the dimensionality of the problem and to extract some properties relevant for the theoretical description of the linear

convection regime. Chapter 4 describes the nonlinear regime, where the two-dimensional nature of the system becomes increasingly important. I compare the results with the experimental study in one-dimensional systems, and give an account of the new phenomena and challenges that a more realistic model of pattern formation in extended systems presents.

1.2 Fundamentals of thermal convection in binary fluid mixtures

Before focusing attention on convection in a binary fluid mixture, I will review the basic instability mechanisms of convection in pure fluids. Since Bénard's turn of the century experiments[15], thermal convection in fluids has become a paradigm for pattern formation, and has attracted the interest of both theorists and experimentalists, because the system's physical mechanisms are well understood, it displays a rich variety of patterns, and the high degree of experimental control allows for detailed comparison between theory and experiment.

To understand the convection instability, consider an infinite layer of fluid confined between two horizontal plates a distance d apart, as illustrated in Figure 1.1. The bottom plate is held at a higher temperature (T_b) than the top plate (T_t). The warmer fluid near the bottom plate is less dense, therefore more buoyant, than the fluid above it. Its tendency to rise is inhibited by dissipation due to viscosity, a kind of fluid friction, and thermal conduction, that quickly destroys the bubble's temperature advantage. Only when the temperature difference between the plates, $\Delta T = T_b - T_t$, exceeds the critical temperature difference, does buoyancy overcome dissipation and the quiescent fluid layer begin to convect. The collective motion of the warmer rising fluid and cooler falling fluid organizes itself into rolls. The associated temperature and refractive index variation can be detected from above by

optical means. When convection first starts, the wavelength of the pattern, the roll pair size, is about twice the layer height. Of course, no real system can be infinite. Most convection experiments are actually performed in narrow rectangular and annular cells. These containers are considered to be one-dimensional systems, because convection rolls, which are parallel to the shorter of the cell's walls, show no relevant variation in the direction parallel to the roll axis. The vertical dependence is also trivial. Therefore, only one spatial dimension, the direction parallel to the long wall and perpendicular to the rolls, is important in the description of convection.

The control parameter that measures external forcing is called the *Rayleigh number*, in honor of Lord Rayleigh who, in 1916, gave the first stability analysis of convection[16]. The Rayleigh number is a dimensionless temperature difference,

$$Ra \equiv \frac{\alpha g \Delta T d^3}{\kappa \nu}.$$

The product of the thermal expansion coefficient (α), gravity (g) and ΔT measures buoyancy's contribution to external forcing, while thermal diffusivity (κ) and kinematic viscosity (ν) gauge dissipation. The critical Rayleigh number at which an infinite layer of pure fluid confined between two rigid plates starts to convect is calculated, using linear stability analysis, to be 1707.76. This is a fundamental property of pure fluids. Once the physical parameters of a particular liquid or gas are known, the critical temperature difference required to start convection in a layer of a given thickness can be precisely calculated.

In binary fluid mixtures, such as the ethanol-water solutions I studied, the presence of a second component leads to richer and more dynamic patterns than those observed in pure fluids. The reason for the greater complexity is that concentration fluctuations dramatically alter the stability properties of the fluid. In liquids concentration fluctuations are very long lived, since the molecular, or mass, diffusion coefficient is two orders of magnitude

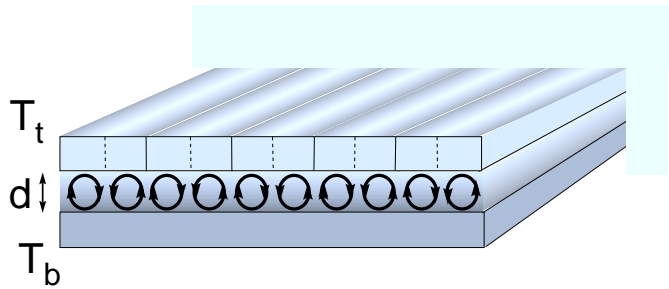


Figure 1.1: Schematic of a convecting fluid layer.

smaller than the thermal diffusion coefficient. Nonequilibrium coupling between fields with vastly different relaxation rates, such as the Soret effect in binary fluids that links mass fluxes to temperature gradients, adds a very slowly relaxing composition dependent term to the buoyancy force. This effect leads to new phenomena not observed in pure fluid convection, such as a backward bifurcation, a bifurcation to time dependent states, the existence of localized states of convection, and states with complex spatio-temporal dynamics. In fact, coupling between temperature and concentration fields is not required in order to see this new behavior — any multicomponent system with vastly different diffusion coefficients, or time scales, may act in a similar way. Some new effects seen in binary fluids are also observed in the thermohaline problem (salt water on top of salt-free water[17]), where the concentration field is independent of the temperature field, and in chemical pattern formation with two diffusing species.

In nonequilibrium systems heat and mass are coupled, so that a gradient in one leads to a flux of the other.* In binary fluid mixtures, the coupling between a temperature gradient and the resulting mass flux, is known as the Soret effect, and it results in the building up of a concentration gradient in response to an applied temperature gradient. There is an equivalent effect describing heat flux generated by a mass gradient, known as the Dufour

*These relationships between generalized forces and fluxes are known as Onsager reciprocal relations

effect, but it is extremely small in liquids and can be safely ignored. The new control parameter in mixtures, the *separation ratio*, is defined as

$$\psi \equiv -\frac{\beta k_T}{\alpha T_0} = -\frac{\beta}{\alpha} S_T \bar{c}(1 - \bar{c}).$$

The separation ratio is a dimensionless number that depends on the thermal expansion coefficient $\alpha = -\frac{1}{\rho}(\frac{\partial \rho}{\partial T})_c$, the solute expansion coefficient $\beta = -\frac{1}{\rho}(\frac{\partial \rho}{\partial c})_T$, the thermodiffusion ratio of the mixture k_T ,[†] and the mean temperature T_0 . The above expression can be rewritten in terms of the Soret coefficient, S_T and the mean alcohol concentration of alcohol \bar{c} , with

$$S_T = \frac{k_T}{T_0} \frac{1}{\bar{c}(1 - \bar{c})}.$$

In ethanol-water mixtures, at reasonable operating temperatures, the separation ratio can take a moderately negative or a positive value. Moreover, as a function of alcohol concentration, see Figure 1.2, ψ attains an absolute minimum, so that the same negative separation ratio can be attained in two different alcohol concentration mixtures. The separation ratio of the mixtures I studied, indicated by pluses in Figure 1.2, was around $\psi = -0.08$.

In ethanol-water mixtures with a negative separation ratio, the Soret effect causes the denser component, water, to migrate to the warmer plate, in this case the bottom plate. This stratification, denser fluid on the bottom and lighter on top, is stable in the gravitational field. Thus, in negative separation ratio mixtures, the Soret effect stabilizes the conduction state against convection, so that the temperature difference required to start convection has to be increased beyond its critical value in a pure fluid. On the other hand, in a mixture with a positive separation ratio, the lighter component migrates to the warmer (bottom) plate, resulting in a destabilizing density gradient. Another consequence of the Soret effect is that it is possible to start a mixture convecting by heating from above. This occurs in negative separation ratio mixtures, since in these fluids the denser component accumulates

[†] $\Delta c = \frac{k_T}{T_0} \Delta T$

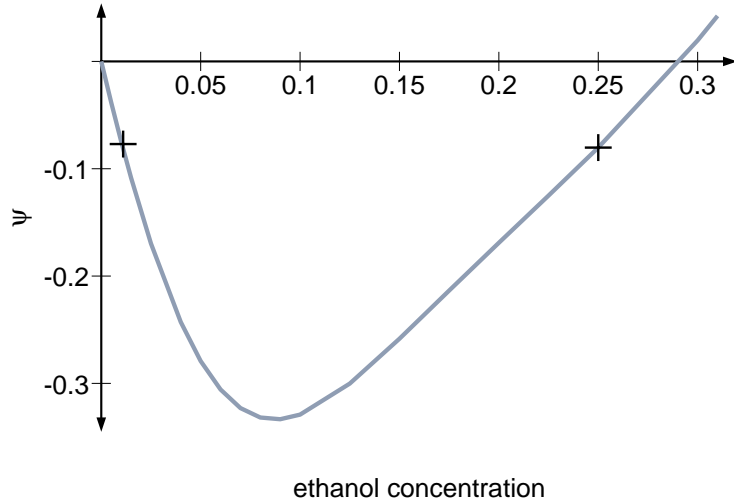


Figure 1.2: Separation ratio vs. concentration (by weight) of alcohol in ethanol–water mixtures, at the mean temperature of 20.5°C . The values were found by fitting data from Kolodner *et al.* [18]. Pluses indicate the separation ratio of mixtures used in the experiments: left plus for a 1.1–wt.% mixture at the mean temperature of 21.4°C , and the right plus is for a 25.0–wt.% ethanol mixture at the mean temperature of 20.5°C .

near the warmer (top) plate, a gravitationally unstable arrangement. The backward bifurcation in $\psi < 0$ mixtures can be explained by the following argument: as soon as convection starts, the stabilizing concentration gradient is destroyed, so that it is preferential for the mixture to convect even more vigorously. This feedback leads the convection amplitude to grow until a steady state of well mixed, large amplitude convection is reached. In this state the well mixed binary mixture acts more or less like a pure fluid. Another important difference with regard to convection in pure fluids is that at onset, convection rolls in a binary mixture travel.

1.3 Theoretical Background

Analytic solutions and numerical simulations of the hydrodynamic equations of motion of a binary fluid mixture in one dimension have shed light on many important stability issues and increased our understanding of pattern formation. Dependence of the critical Rayleigh number on the separation ratio, the value of critical wave vector, competition between standing and traveling waves, even the existence and stability of localized states can be found by examining the equations of motion of the fluid, or the coarse-grained amplitude equations. By one-dimensional systems I mean simply the narrow fluid containers used in convection experiments, such as rectangles and annuli. As explained in the preceding section, in such systems only one direction, one that is parallel to the long wall, is important in the description and the solution of the problem. The other two spatial directions, vertical and parallel to the rolls, are considered trivial. Vertical solutions depend only on the vertical boundary conditions, and structures parallel to the rolls show no variation, apart from the expected boundary layer effects. In wide cells, the so called two-dimensional systems, variation in both horizontal dimensions must be taken into account. In two dimensions the solutions of the equations of motion are analytically intractable and numerically too intensive for present computational methods, especially for larger systems. In a sense, the physical system itself solves the equations and finds stable solutions. It is not my intention to go into the details of the solution of the fluid equations, which can be found in the standard treatments[19, 17]. Rather, I want to sketch the approach physicists use to study the instabilities in pattern forming systems. My treatment of this problem is modeled after a Diplomarbeit (Master's Thesis) of Wolfgang Schöpf[20].

1.3.1 Equations of motion of a two component fluid

The hydrodynamic equations of motion of the fluid describing three coupled fields, the velocity, temperature and concentration fields, are approximately given by

$$\vec{\nabla} \cdot \vec{v} = 0 \quad (1.1)$$

$$\frac{\partial \vec{v}}{\partial t} + (\vec{v} \cdot \vec{\nabla}) \vec{v} = -\frac{\vec{\nabla} p}{\rho_0} + \nu \nabla^2 \vec{v} + \frac{\rho}{\rho_0} \vec{g} \quad (1.2)$$

$$\frac{\partial T}{\partial t} + (\vec{v} \cdot \vec{\nabla}) T = \kappa \nabla^2 T \quad (1.3)$$

$$\frac{\partial c}{\partial t} + (\vec{v} \cdot \vec{\nabla}) c = D \nabla^2 c + DS_T c_0 (1 - c_0) \nabla^2 T. \quad (1.4)$$

Here ρ_0 , c_0 , and T_0 are the reference density, concentration and temperature at the top plate. The above equations express conservation laws of the relevant quantities. The first equation, Equation 1.1, is the continuity (mass conservation) equation for an incompressible fluid. The Navier–Stokes equation, Equation 1.2, describes the conservation of momentum, while the heat flux equation, Equation 1.3, expresses conservation of energy. The term giving rise to the Dufour effect, the counterpart of the Soret effect, that describes the coupling between concentration gradient and heat flux, is absent from equation 1.3, because this effect is negligible in liquids. The continuity equation for one of the mixture components, Equation 1.4, in this case alcohol conservation law, contains the Soret effect term in addition to the diffusion term ($\nabla^2 c$).

Together with the equation of state, relating fluid density to other parameters, these equations can be applied to a broad range of fluid behaviors, from quiescent, purely diffusing fluids to turbulent flow. By choosing the appropriate conditions in the equation of state, one can restrict the scope of the equations to be applicable only to certain classes of problems. For incompressible fluids, like pure liquids and mixtures, the Oberbeck-Boussinesq approximation is appropriate. This approximation holds that density varia-

tions are only important in the driving buoyancy term, and are given by

$$\rho = \rho_0[1 - \alpha(T - T_0) + \beta(c - c_0)]$$

α and β are the thermal and solute expansion coefficients defined earlier. Moreover, all fluid parameters are independent of temperature in this approximation. The Oberbeck-Boussinesq approximation is a good approximation for a broad range of experimental conditions, especially for liquids at room temperature, where fluid parameters change a few percent over the temperature difference of several degrees required to start convection. The approximation breaks down in very thin convection layers, where temperature differences on the order of $\Delta T_c \approx 40^\circ\text{C}$ are required to drive convection. If a less restrictive equation of state is used with the fluid equations, the stability properties of the system change significantly. In such non-Boussinesq fluids, a hexagonal pattern is observed at convection threshold[8], instead of a roll pattern.

The equations of motion are usually written not in the form given by Equations 1.1–1.4, but in a dimensionless form in which space is normalized by the fluid layer thickness, d , time is normalized by the vertical thermal diffusion time d^2/κ , and the physical properties of the fluid are fully characterized by the dimensionless parameters, Prandtl number $Pr = \nu/\kappa$ and Lewis number $Le = D/\kappa$, in addition to the control parameters Rayleigh number and the separation ratio.

1.3.2 Linear stability analysis

Below the convection threshold the equations of motion in the Boussinesq approximation have well known conduction solutions: velocity is zero everywhere and temperature and concentration have linear vertical profiles, typical of purely diffusive fields. The next step in the theoretical analysis is to examine what happens to infinitesimal perturbations away from the conduction

solution just above the convection threshold. The choice of boundary conditions dictates the form that solutions of the problem take. While idealized boundary conditions, periodic and free, are the simplest boundary conditions from a theoretical point of view, the equations can also be solved for the more realistic boundary conditions, that is rigid and impermeable boundaries.

Solution to the fluid equations close to the convection threshold can be written as a sum of the base state (conduction) solution and infinitesimal perturbations. The equations of motion are then linearized, that is nonlinear terms, which are higher order in perturbations, are dropped. Infinitesimal perturbations with a wavevector q are assumed to have an exponential growth rate $\sigma(q)$. At this point it is useful to introduce a slightly different control parameter:

$$\epsilon \equiv \frac{Ra - Ra_c}{Ra_c}.$$

ϵ is defined as distance away from the critical Rayleigh number. For $\epsilon < 0$, in the conduction state, the growth rate of the perturbations is negative (*i.e.* $\text{Re}\sigma(q) < 0$); they decay and the system returns to the conduction state. For $\epsilon > 0$, the growth rate of the perturbations is positive, and the conduction state is unstable to a state with convection. If $\text{Im}\sigma(q) \neq 0$, the convection state has an oscillatory time dependence. The linearized equations of motion are solved for the growth rate and many stability properties of the system are calculated, such as the separation ratio dependent suppression of the convection threshold, Figure 1.3, and the critical wavevector of the pattern. For sufficiently negative ψ , convection solutions are also found to be oscillatory in time just above onset, and the critical oscillation frequency, the Hopf frequency, can be calculated using linear stability analysis.

1.4 Amplitude equation

Slightly above onset, for $\epsilon \ll 1$, nonlinearities are weak, and spatial and temporal modulations of the basic spatially periodic, and perhaps time oscil-

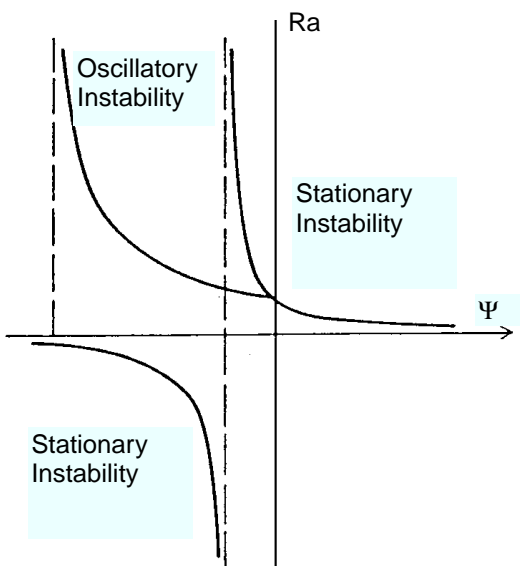


Figure 1.3: Schematic of the results of linear stability calculation of the critical Rayleigh number *vs* ψ for binary-fluid mixtures, from reference [21].

latory, pattern are slow. A perturbative expansion in ϵ leads to a very simple equation, known as the Ginzburg–Landau (GLE), or amplitude, equation for the slowly varying envelope of the basic pattern. While the GLE can be derived directly from the equations of motion describing thermal convection in fluids[22, 23], it is quite general and can be applied to many classes of continuous extended systems. There is only a small number of amplitude equations “whose form is *universal*[‡] and whose numerical parameters reflect the details of each physical system” [24]. Which form the equation takes depends on the particular linear instabilities that describe the system. Thus, the GLE describes stationary, spatially periodic patterns, like the ones observed in pure fluid convection, while the complex GLE applies to oscillatory patterns in a binary fluid convection. For systems in which the microscopic physics is not

[‡]“Universal” is used here in the usual sense of the word, meaning that the expression can be applied to classes of systems regardless of the details of microscopic physical interactions.

fully known, symmetry considerations alone can dictate the form of the phenomenological amplitude equation. Constraints of brevity prevent me from going into as much depth as the topic of amplitude equations warrants. My aim in this section is to provide the reader with an understanding, however sketchy, of the nature of this mythical amplitude. For a far-reaching and concise exposition of the amplitude equation approach to pattern formation in a variety of systems, I refer the reader to Cross and Hohenberg’s review[24], from which I borrow some of my insights.

The motivation behind the derivation of the amplitude equation is the recognition that convective fields, such as vertical fluid velocity and temperature fields, can be separated into dependencies on “fast” variables, the usual space and time (\vec{x}, t) coordinates, and “slow” variables (\vec{X}, T) . The slow variables describe the slow modulation of the fast variable and are related to them by: $X = \epsilon^{1/2}x$, $Y = \epsilon^{1/4}y$, $T = \epsilon t$. This separation is valid as long as ϵ is small and can be used as an expansion parameter. Implicit in the amplitude equation formalism is an assumption that convection rolls are everywhere perpendicular to the x-axis. In fact, once convection breaks the orientational symmetry of an isotropic system, roll orientation may vary only as $O(\epsilon^{1/4})$. With this caveat, the most unstable mode of the convection field in the oscillatory instability can be written as a superposition of right and left traveling rolls, all of which are perpendicular to the x-axis,

$$U(\vec{x}, t) = U_0 \left[A_R(X, Y, T) e^{i(q_c x - \omega_c t)} + A_L(X, Y, T) e^{-i(q_c x + \omega_c t)} \right] + \text{c.c} + O(\epsilon) \quad (1.5)$$

Vertical dependence of the field is hidden in the U_0 term. In the above expression, I explicitly wrote the amplitudes A_R and A_L as functions of the slow variables to emphasize that they produce the envelope of the pattern. The basic pattern is described by exponentials in the above expression as modulations in space and time at the critical wave vector and frequency. The dynamics of the envelope are described by two coupled complex Ginzburg-Landau equations (CGLE), one for each of the amplitudes. For simplicity,

the one-dimensional case is considered first.

$$\begin{aligned}
\tau_0 [\partial_t A_R + s_0 \partial_x A_R] &= \epsilon(1 + ic_0)A_R + \xi_0^2(1 + ic_1)\partial_x^2 A_R - g_0(1 - ic_3)|A_R|^2 A_R \\
&\quad - g_1(1 - ic_2)|A_L|^2 A_R \text{ for right TW} \\
\tau_0 [\partial_t A_L - s_0 \partial_x A_L] &= \epsilon(1 + ic_0)A_L + \xi_0^2(1 + ic_1)\partial_x^2 A_L - g_0(1 - ic_3)|A_L|^2 A_L \\
&\quad - g_1(1 - ic_2)|A_R|^2 A_L \text{ for left TW}
\end{aligned} \tag{1.6}$$

The coefficients τ_0 , ξ_0 , and g_0 set the scale for the slow time, space and amplitude variations, while q_c and ω_c set the scales of the fast space and time variations. The group velocity is $s_0 = \left. \frac{\partial \omega}{\partial q} \right|_{q=q_c, \epsilon=0}$. These quantities contain the physical characteristics of the system and the coefficients of the linear terms can be computed from the linear stability analysis. In particular,

$$\frac{1}{\tau_0} = \left. \frac{\partial \sigma(q)}{\partial \epsilon} \right|_{q=q_c, \epsilon=0}$$

and

$$\frac{\xi_0^2}{\tau_0} = -\frac{1}{2} \left. \frac{\partial^2 \sigma(q)}{\partial q^2} \right|_{q=q_c, \epsilon=0},$$

where $\sigma(q)$ is the growth rate of the pattern. The quantity $\xi_0/\sqrt{\epsilon}$ governs the rate at which convection spreads spatially. Appearance of odd powers of the amplitude in Eqn. 1.6 is suggested by considerations of the amplitude reversal symmetry: the invariance of the system under the transformations $A \rightarrow -A$. The physical reason for this symmetry is that in Boussinesq fluids the up- and down-flowing regions of fluid are completely equivalent. Failure of the up-down reversal symmetry, as in non-Boussinesq fluids, where the upflowing regions have physical properties that are different from those in the downflowing fluids, results in an amplitude equation with nonlinear terms that are even powers of A . This results in a different bifurcation and pattern forming behavior.

The two limits of the CGLE

There is a number of interesting points to be raised about the complex Ginzburg-Landau equations, Eqns. 1.6. First, if just a single amplitude is taken (no cross coupling terms) and all the imaginary coefficients, as well as the propagation term $s_0 \partial_x A$, are set to zero, then a one-dimensional GLE is recovered. This equation describes the dynamics of the amplitudes of patterns in pure fluid convection, for example. It also describes the behavior of the order parameter near the critical point in equilibrium phase transitions. A second important property of the Ginzburg-Landau equation is that it has a potential and, therefore, can be rewritten in a variational form

$$\tau_0 \frac{\partial A}{\partial t} = -\frac{\delta F}{\delta A^*}, \quad (1.7)$$

where F is the potential, akin to the free energy in thermodynamics physics, and A^* is the complex conjugate of the amplitude. In other words, the amplitude obeys relaxational dynamics, and the system evolves to a steady state that minimizes the potential. Once it is known that a potential exists, the steady state of the system can be uniquely specified. This is also true of equilibrium systems. When the intensive parameters of an infinite equilibrium system are kept fixed, two phases, e.g. ice and water, can coexist only at a unique value of the control parameter. Away from this value, only one phase is stable, and the system evolves to a steady state that consists of only that one phase. This is not true of binary-fluid convection, when the CGLE is relevant, and this leads to the existence of novel localized states of convection.

If, instead, one takes the complex GLE in the limit of very large imaginary coefficients, one recovers the non-linear Schrödinger equation. This equation is one of the few that describe integrable dispersive nonlinear systems that have stable localized solutions, known as solitons[25, 26]. Solitons are robust solitary structures that have the remarkable property that, in spite of dispersion, they manage to preserve their shape and size during interactions

with each other and the system. This property is borne of a delicate balance between the effects of nonlinearities and dispersion in these systems. Solitons have been widely investigated in many systems for their technological utilization, such as their ability to travel long distances with minimal degradation or shape change. Most physical systems are also dissipative in addition to being dispersive. Discovery of pulses in binary–fluid convection[27, 28] and of localized solutions in the 1d quintic complex GLE[29], showed that soliton-like structures exist even in dissipative systems.

The amplitude equations also describe bifurcations in dynamical system, that is the response of the system to the stress parameter as it crosses its threshold. When the coefficient of the first nonlinear term, g_0 , is positive, the amplitude of the steady states above convection threshold grow as $A = \sqrt{\epsilon/g_0}$. A continuous change of the order parameter with variation of the control parameter is a signature of a forward bifurcations. If, on the other hand, the coefficient of the cubic term, g_0 is negative, an additional quintic nonlinear term is needed to saturate the amplitude growth. In this case, the bifurcation is said to be a subcritical, or backward, bifurcation. In convection experiments it is customary to display the Nusselt number diagram instead of the bifurcation diagram. The Nusselt number measures the total heat transported through the cell (i.e. by convection and conduction) with respect to the heat transported by conduction alone. As a measurement of heat, or dissipated power, it is an easy parameter to measure, but it is also the spatially averaged product of temperature and velocity fields; therefore, the Nusselt number is proportional to the square of the convection amplitude.

Amplitude equation in two dimensions

To obtain a two dimensional form of the complex Ginzburg–Landau equation Eq. 1.6, one that still describes rolls whose wave vector points in the x–

direction, the diffusive term, ∂_x^2 becomes[22, 23]

$$\left(\partial_x - \frac{i}{2q_c}\partial_y^2\right)^2 \quad (1.8)$$

and the group velocity term $s_0\partial_x A$ is transformed into[30, 21]

$$s_0 \left(\partial_x - \frac{i}{2q_c}\partial_y^2 + \frac{1}{2q_c^2}\partial_x\partial_y^2 - \frac{i}{8q_c^3}\partial_y^4 \right) \quad (1.9)$$

Brand *et al.*[21] show that in two spatial dimensions, a wave train whose envelope satisfies the 2d complex Ginzburg–Landau equation is most unstable to perturbations that are transverse to the direction of wave propagation. Moreover, waves with a wave vector $\vec{q} = (q_c, 0)$ are unstable to a Benjamin–Feir type side band perturbation with a wave vector $\vec{K} = (q_c - (\epsilon/2q_c)K_y^2, \sqrt{\epsilon}K_y)$. It is known from the work of Benjamin and Feir[31] that a wave train of finite amplitude deep water waves with a frequency ω is unstable to being modulated at a low frequency, resulting in a wave train with a frequency $\omega(1 \pm \delta)$. The effects of both dispersion and nonlinear coupling between the modes, transfer the energy from the primary mode to the side bands with $0 < \delta \leq \sqrt{2}qa$, where q is the wave number of the fundamental mode, and a is the amplitude of perturbations. As the side band modes grow, an initially monochromatic wave train will in time lose coherence and become highly irregular.[§] In a similar way, the competition between all modes of a destabilized traveling wave train in binary fluids leads to an irregular convective flow, that Brand *et al.* name Benjamin–Feir turbulence[21]. This turbulence is more pronounced in wide two-dimensional convection cells than in narrow cells.

The condition for the transverse Benjamin–Feir type instability, that can be derived for the quintic order CGLE, appropriate for systems with a sub-

[§]This explains why deep water waves are observed as wave packets and never as monochromatic wave trains.

critical bifurcation, is [24],

$$s_0 \frac{\partial \omega}{\partial |A|} \frac{\partial |A|}{\partial \epsilon} < 0. \quad (1.10)$$

This condition is satisfied by binary fluid mixtures, whose traveling wave frequency decreases as the amplitude increases with ϵ . The frequently observed tendency of the convection rolls to become unstable to perturbations perpendicular to the direction of wave propagation during the nonlinear regime (see chapter 4) could be a manifestation of the transverse Benjamin–Feir instability.

The complicated form of the derivative terms, especially the group velocity, makes finding analytic solutions of the 2d complex Ginzburg–Landau equation a very challenging task. For example, it is not known whether the 2d CGLE has pulse solutions like the 1d equation. Solitons, the analogs of pulses, are known to be unstable in the less general two-dimensional nonlinear Schrödinger equation. Though in time, it might be computationally feasible to search the parameter space of the CGLE for localized solutions, the experimental search for localized pulses of convection has to proceed without theoretical guidance.

In addition to the amplitude equation, another model equation has been proposed by Swift and Hohenberg[32] for the study of pattern formation in extended system. This order parameter equation is constructed to be rotationally invariant, unlike the GLE in two dimensions, and it contains the full spatio–temporal dynamics of the patterns near onset, not just the slow amplitude dynamics. Solutions of the order parameter equation constructed to resemble a system with a backward Hopf bifurcation, exhibit structures reminiscent of the patterns observed in wide rectangular and cylindrical cells[33] and localized convecting regions that somewhat resemble pulses[34]. Unfortunately, no direct connection has been made between the parameter range for which the order parameter model shows appropriate behavior, and the experimental parameters.

1.5 Experiments on binary–fluid convection

Early experimental observations of the oscillatory nature of the convection threshold in binary–fluid mixtures[35, 36] indicated that an ideal paradigm for the study of dynamical systems had been found. Unlike pure fluids, which exhibit time dependent behavior only for very high values of the control parameter, convection in binary fluids is already dynamic at onset, giving hope that a theoretical description of these dynamics is possible. To date there has been much progress in understanding the linear properties of this system in one spatial dimension, and also in the understanding of surprising new states, such as the localized pulses of traveling wave convection and “dispersive chaos”. A linear stability analysis of the full equations of motion correctly predicts the onset of convection, wave vector, and other properties. In many cases it is possible to perform a perturbation expansion about the base conducting state to generate a greatly simplified equation for the amplitude of the convective flow. Amplitude equations have proved useful in understanding many fundamental behaviors of this dynamical system. However, extending them to two dimensions has proved to be a challenge. In subsequent chapters I will show how taking advantage of the system’s symmetries allows for comparison of convective behavior in a two-dimensional system with the one-dimensional systems, represented by narrow rectangular and annular cells, that have been extensively studied experimentally and explained theoretically.

1.5.1 Linear transients of TW convection

Linear transients of traveling–wave convection have virtually the same character (onset, wavevector, critical, or Hopf, frequency) in both rectangular and annular geometries. In rectangular cells, however, the presence of reflecting end walls leads to the existence of counterpropagating linear waves, whereas in the annular cells the waves can be made unidirectional[37]. In the

cylindrical convection cells I studied, the waves travel in the radial direction and reflect from the side wall. Therefore, these systems are analogous to rectangular containers. I discuss below some of the results of experiments on linear transients in narrow rectangular containers.

Experimental observations of linear and weakly nonlinear TW

At the convection threshold, convection starts to grow uniformly over the entire cell in the form of linear transients. In narrow rectangular cells, convection rolls line up with the short side wall and propagate in the direction perpendicular to it. Right TW are visible in the right half of the convection cell, left TW visible in the other half, and a standing wave is present in the middle. The shadowgraph signal of the TW was fit well by functions that closely resemble solutions of the CGLE[38]. Using complex demodulation, it is possible to decompose these waves into right and left TW[39]. Counter-propagating waves grow exponentially in space as they pass through the cell and are reflected with loss by the end walls[40]. The reflection coefficient can be computed simply by taking the ratio of the wave amplitudes at the walls. When the control parameter is increased slightly, linear transients evolve into a “blinking” state[40, 41]. During this transient, right TW appear periodically in the right half of the cell, and half a “blinking” period later, left TW are visible in the left half. Demodulation of the signal shows that the profiles of the right and left TW are no longer symmetric as in the linear regime, but alternate between one being strong with the other one suppressed, and *vice versa*. The TW frequency of the “blinking” state is reduced from its linear value. The state’s character is sensitive to cell size and experimental conditions[42].

In wider rectangular cells, nonlinear states focus in the direction perpendicular to the propagation direction, that is they become narrow and recede from the long walls[42, 43]. This is already seen in a $1 \times 4.9 \times \Gamma$ cell. Some of the aspects of the linear and nonlinear TW transients observed in narrow

rectangular channels have also been observed in wide (2-dimensional) convection cells and, therefore, seem to be general in nature. These features include the observation that linear transients are a superposition of counter-propagating waves that grow spatially as they travel through the cell and are reflected with loss by the end walls. Focusing of the convection rolls in the direction perpendicular to wave propagation is especially striking in a circular cell. These transients will be discussed at length in the last two chapters of this thesis.

Theoretical analysis of linear TW

Coupled cubic order complex Ginzburg–Landau equations without diffusion and dispersion terms correctly capture the behavior of linear and weakly nonlinear traveling waves in binary fluid mixtures close to threshold [45, 46, 42, 40]. Therefore, a simplified linear CGLE will be considered here in relation to the linear properties of TW. The theory cannot be extended to the fully nonlinear case, e.g. to describe the steady cell–filling convective state, because the solutions in that case cannot be considered to be weak perturbations of the base conduction state. Propagating solutions of the CGLE can be written as [47, 45, 46]

$$\begin{aligned} A_R &= a_R e^{\epsilon x/s_0} e^{i(Kx - \Omega_K t)} && \text{for the right TW,} \\ A_L &= a_L e^{-\epsilon x/s_0} e^{-i(Kx + \Omega_K t)} && \text{for the left TW.} \end{aligned} \tag{1.11}$$

Traveling waves are reflected with loss by the end walls at $x = \pm\Gamma/2$. The coefficient of reflection, $\gamma = |\gamma|e^{i\phi_\gamma}$, can in principle be complex. K and Ω_K are the wavevector and frequency of the slow amplitude variations. In other words, they represent the deviations of the pattern’s wavevector and frequency from their critical values (see Eqn. 1.5). The boundary conditions incorporating reflection of the physical waves at $x = \pm\Gamma/2$ are

$$\begin{aligned} A_L(\Gamma/2)e^{-iq_c\Gamma/2} &= \gamma A_R(\Gamma/2)e^{iq_c\Gamma/2} \\ A_R(-\Gamma/2)e^{-iq_c\Gamma/2} &= \gamma A_L(-\Gamma/2)e^{iq_c\Gamma/2}. \end{aligned} \tag{1.12}$$

Solving separately for the real and imaginary parts of the boundary conditions above, leads to,

$$a_R = \pm a_L,$$

and the quantization condition on the wave vector $K = O(\Gamma^{-1})$ of the slowly varying amplitude,

$$(q_c + K_n)\Gamma + \phi_\gamma = n\pi,$$

where n is an integer. Note that when n is even, $a_R = a_L$, and when n is odd, $a_r = -a_L$. K_n forms a discrete set of wavevectors, or modes. A single mode, one with the smallest threshold ϵ_s , grows at onset. If, however, two different modes have the same threshold, both will grow and the resulting pattern represents the superposition of the modes. The beating of two linear modes at the convection threshold has been studied experimentally[48].

The presence of reflecting side walls in a finite system shifts the convection threshold away from its critical value in an infinite system. In the linear stability analysis, the threshold shift can be estimated by balancing amplitude loss due to reflections with its growth due to passage through the convection cell and is given by

$$\epsilon_s = \frac{s_0}{\Gamma} \ln \left(\frac{1}{|\gamma|} \right) + O(\Gamma^{-2}). \quad (1.13)$$

The $O(\Gamma^{-1})$ shift in threshold has been experimentally confirmed in narrow rectangular cells[48]. Other effects, such as the linear shift in Ω_K , leads to higher order corrections to ϵ_s .

Solutions of the CGLE represent a pair of traveling waves whose envelopes grow as the waves travel through the cell. Reflection of the wave at the end wall feeds the oppositely propagating wave. The amplitude of right TW is large in the right half of the cell, and the oppositely propagating wave amplitude is large in the left half. Superposition of these two waves lead to a standing wave in the middle of the cell, where the amplitudes are equal. This agrees with experimental observations of linear TW in rectangular cells[27, 40, 49].

Numerical studies of nonlinear TW

Nonlinear traveling waves and stationary cell-filling convection rolls cannot be adequately described by the amplitude equations. Lücke and coworkers[50, 51] investigated these states by numerically integrating the hydrodynamic equations of motion. They were also able to visualize convective fields and, in particular, elucidate the important role of the concentration field. It significantly influences stability properties of convective structures and causes a variety of dynamical behaviors by coupling to the temperature field via the Soret effect and by contributing to the buoyancy force.

In the nonlinear TW state, a profound asymmetry exists in the vertical cross-sectional plane between the oppositely circulating regions that make up the convection roll pair — they are shifted alternately to top and bottom plates. For negative separation ratio mixtures, an alcohol-rich layer near the top plate feeds one of the rolls, while an alcohol-poor layer at the bottom plate feeds the other member of the pair of rolls, with little mixing. While temperature and vertical velocity fields are harmonic, like those in a pure fluid, they are phase shifted with respect to one another. This phase shift grows with the wave's phase velocity, and it drives a lateral heat current. Likewise, there is a phase shift between the strongly anharmonic concentration field and vertical velocity field, that drives a lateral concentration current. The lateral currents circulate in the direction parallel to the phase velocity of the rolls in the top half of the cell and antiparallel to the phase velocity in the bottom half of the cell, so that the net current is zero. As the TW phase velocity decreases, rolls become more mirror symmetric about their midplane. Concentration is quickly homogenized by mixing in the symmetric state, so that at zero phase velocity, in the stationary overturning convection state, the mixture is indistinguishable from a strongly convecting pure fluid. There are no lateral heat or concentration currents in this state.

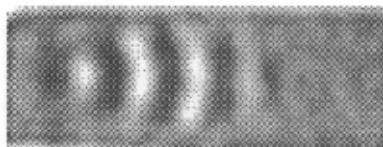


Figure 1.4: Localized pulse of traveling wave convection from Heinrichs *et al.*[27] Only the section of the cell containing the pulse is shown.

1.5.2 Localized pulses of convection

The complex Ginzburg–Landau equation 1.6 has some striking properties. The most important of these might be that it does not have a potential and, therefore, cannot be written in variational form. This leads to the possibility of a coexistence of two phases, conduction and convection, over a finite range of the control parameter. Such states have indeed been observed in binary–fluid experiments in narrow rectangular[27, 43] cells. One such pulse[43], seen in a rectangular cell of length $25.3d$, width $4.87d$ and depth $d = 0.308$ cm filled with a 25% ethanol in water binary–mixture with a separation ratio $\psi = -0.08$, is illustrated in Figure 1.4. It consists of a short train of traveling convection rolls, surrounded by a quiescent fluid. In wider cells, pulses take on a characteristic curved shape, that led to the nickname “football.” The rolls are curved slightly in the direction of wave propagation, because nonlinear effects decrease TW frequency in places where the convection amplitude is large, and vice versa. Since the convection amplitude has to go to zero at the edge of the pulse, the waves are traveling fastest there, giving the pulse its curved shape.

Experimental observations of pulses

Localized pulses of traveling-wave convection (LTW) have been observed to have essentially the same features in both rectangular and in narrow annular cell geometries[49]. The transverse aspect ratio of the rectangular cells in which stable LTW have been studied ranges up to $4.87d$ [27]. Stable pulses

have been observed and studied for a wide range of negative separation ratios, from $-0.253 \leq \psi \leq -0.005$ [27, 28, 40, 41]. For moderately negative separation ratios $\psi \leq -0.07$, they are the first steady convecting state seen above onset, evolving directly from the linear TW transient[27, 43, 49, 52, 53]. For less negative separation ratios, $-0.058 \leq \psi \leq -0.005$, linear counterpropagating waves in rectangular cells lead to an asymmetric, temporally modulated “blinking” state[41, 40, 54], where TW of appreciable amplitude alternate between being confined at one end of the cell or the other. “Blinking” states have a characteristic frequency that drops steadily as ϵ is increased. Steady localized pulses form at the value of ϵ for which the “blinking” frequency reaches zero[40]. In addition to localized pulses, confined states of arbitrary length are also observed in one– dimensional cells[55, 56]. They are stable for $\psi \leq -0.167$, and unstable for $\psi \gtrsim -0.13$, though because they have a strongly ϵ -dependent spreading rate, they may be maintained in a steady state by modulating the control parameter to keep the expansion rate zero[56].

Many of the structural, propagation, and stability properties of pulses have been experimentally studied, and shown to agree qualitatively in some cases with theoretical predictions. LTW are observed to have a unique width, $\approx 5d$, that depends only weakly on experimental parameters[49, 55], a slow drift of the envelope[57, 58], and stability over a wide range of the control parameter that extends in some cases to positive ϵ . The frequency of the underlying traveling waves is about half of the Hopf frequency. The slow drift velocity of the envelope of the pulse increases monotonically with distance ϵ from threshold at fixed ψ , and decreases monotonically with ψ at fixed ϵ [58]. As a matter of fact, the drift velocity depends so sensitively on the local stress parameter $\epsilon(x)$, that Kolodner used it as a measure of a cell’s ϵ inhomogeneity, that he then corrected with an array of adjustable heat sources[57]. It has been possible to create more than one pulse in an annular container, either by letting it form spontaneously or by launching disturbances. Interactions

and collisions between counterpropagating pulses have been studied to some degree[59], in the hope of making connection with theory.

One of the more puzzling aspects of pulses is their stability at positive ϵ . The expectation is that for $\epsilon > 0$, the conducting region that surrounds the pulse will start to convect and fill the cell with convection, destroying the pulse in the process. Pulse solutions of the CGLE are stable only for $\epsilon < 0$ [60]. Instead, pulses are destabilized only at high values of the control parameter, for example in a $\psi = -0.08$ mixture, the stability range is $-0.016 \leq \epsilon \leq 0.008$ [49]. Three mechanisms are observed to be responsible for the destabilization of pulses. The first mechanism is intimately related to their stability for $\epsilon > 0$. It was observed that localized states absorb linear TW of small amplitude[52]. In other words, pulses suppress fluctuations of the conduction state, stabilizing it against convection. However, linear waves of large enough amplitude may destroy the pulse. Spontaneous fluctuations that are convectively amplified by the passage through the cell, can grow to the critical amplitude in a long enough experimental cell at which the transition to a cell filling state is triggered. The threshold for fluctuation-mediated destabilization of pulses can be calculated from a linear stability analysis,

$$\epsilon_f = \frac{s_0 \tau_0}{\Gamma} \ln \gamma_f,$$

where s_0 , τ_0 and Γ are the familiar group velocity of the linear TW, time scale governing amplitude growth, and the dimensionless length of the convection cell, respectively. γ_f , the critical gain factor of the TW during their passage through the conducting fluid, is measured in the experiments to be 40–400. With this gain factor, in an annular cell of length $\Gamma = 80.1$, ϵ_f is between 0.009 and 0.014[52]. When this fluctuation threshold is exceeded, convection grows in the quiescent region surrounding the pulse, leading to a cell-filling transition. In annular cells with multiple pulses, this transition is shifted to a higher control parameter, the presence of absorbing pulses effectively reducing the length over which fluctuations may grow. In a cell with a high

fluctuation threshold, pulses lose stability by another mechanism long before ϵ_f is reached[53].

The second pulse destabilization mechanism is the transition from a convective to an absolute instability. The absolute instability threshold is the point at which propagating perturbations spread at a faster rate than they can be swept out of the system by propagating, causing these perturbations to grow at any fixed position in the cell. Balancing the rates of growth and propagation in the linear stability analysis, leads to the absolute instability threshold for the infinite system

$$\epsilon_a = \left(\frac{s_0 \tau_0}{2\xi_0} \right)^2,$$

where ξ_0 sets the scale of spatial variations of the amplitude. Linear analysis correctly predicts the destabilization threshold for fixed width localized pulses[61, 56].

The third and last destabilization mechanism of confined states in narrow experimental cells is an “intrinsic” destabilization. Pulses grow by front propagation when this “intrinsic” destabilization threshold is exceeded[56]. For large magnitude negative separation ratios this destabilization occurs at subcritical ϵ .

The final important remark to be made about experimental studies of localized states is that they cause a large-scale concentration redistribution in the cell[62, 81]. Since the vertical concentration distribution is intimately tied to the buoyancy forces, it significantly influences the stability of the conduction state. It is precisely this large scale concentration flux that stabilizes the localized states[64, 51], as will be discussed below.

Theoretical investigations of localized states

Theoretical approaches have yielded useful models for the study of localized states, but they have had mixed success in explaining many of their

experimentally observed features. Evidence of large scale concentration redistribution suggests that localized states cannot be treated as infinitesimal perturbation of the base conducting state, an approach taken by amplitude equations. Despite the fact that there is no clear range of validity for the amplitude equation application to the study of localized states, the complex Ginzburg–Landau equation has been investigated on a number of fronts in relation to pulses. The CGLE is an attractive model, because it can be derived from first principles for binary fluid convection[65, 66, 67], and all of its linear, and some of its nonlinear, coefficients can be computed directly from the physical fluid parameters and measured experimentally. Other phenomenological amplitude equations, including an extension of the CGLE that incorporates a slow concentration mode[68], have also been applied to the problem, making many successful predictions of such pulse properties as its shape and slow drift velocity.

Perhaps the most important theoretical result is that the CGLE has pulse solutions near a subcritical bifurcation[29, 69, 70, 60, 71]. These solutions fit the narrow pulses well in both rectangular and annular cell geometries, albeit with adjustable parameters[49]. This model also predicts an envelope drift, which was at first not measured. Before the pulses were shown to be intrinsic and stable solutions of the CGLE, numerical simulations of coupled GLE in the presence of end wall reflections reproduced some experimental features[47, 44]. This led, incorrectly, to the claim that end wall reflections stabilize pulses. Collisions between pulses have been studied theoretically using a phenomenological coupled supercritical CGLE[72]. These studies fail to reproduce experimental observations even qualitatively.

Numerical integration of the full hydrodynamic equations[64, 51] has resulted in one of the most fruitful approaches to the problem. It has not only yielded predictions that are in good qualitative agreement with the measurements of the shape and drift velocity of the localized pulses and the confined states of arbitrary length[64, 58], but it has also enabled the visualization of

the convective currents, settling finally the issue of pulse stability. Localized TW states cause a large scale concentration current, that flows in the direction parallel to the phase velocity of the waves in the top half of the cell and in the opposite direction in the bottom half. Thus, concentration builds up ahead of the pulse in the top portion of the cell and is depleted in the bottom portion of the cell. The resulting increase in the stabilizing vertical concentration gradient weakens the buoyancy forces ahead of the pulse, enhancing the stability of the conduction state there. In a sense, the pulse builds up a concentration “barrier” ahead of itself that inhibits convection’s invasion of the quiescent region. Despite many nice results, however, some observed features, such as the ϵ dependence of the drift velocity, have not yet been quantitatively explained even by numerical studies of the full equations of motion.

1.5.3 Spatio–temporal complexity

As the control parameter is increased, a pattern forming system typically undergoes a series of transitions from a trivial base state, to one with a steady or a time–periodic pattern, to a state with increasingly complex spatio–temporal dynamics, to full blown turbulence at very large values of the control parameter. Systems that show complex spatio–temporal dynamics close to threshold, e.g. spiral chaos in gases[9] and Faraday instability of a parametrically oscillated fluid layer[5], are good candidates for theoretical modeling, since great strides in the understanding of pattern formation close to threshold have been made. Observation of dynamical states with increasing spatio–temporal complexity in binary–fluid convection in a narrow range of a control parameter above threshold, present yet another candidate for the study of systems exhibiting chaotic dynamics. Wide two-dimensional systems with an extra degree of freedom have a potential to exhibit new phenomena that might contribute to understanding spatio–temporal complexity.

During the regime where “blinking” behavior is observed in weakly non-linear convection in rectangular cells, convection in narrow annuli shows an erratic bursting behavior[37, 73, 74, 75], characterized by “erratic, repeated appearance and subsequent abrupt decay of spatially localized bursts of TW” convection[74]. As ϵ is increased, the frequency of these bursts, as well as their spatial density, grows until, at $\epsilon = 1.11 \times 10^{-2}$, there is a transition to steady persistent convective region occupying a portion of the cell. The size of this region increases linearly until, at $\epsilon = 1.92 \times 10^{-2}$, the cell fills with steady rolls. Bursting behavior was first studied in specially prepared unidirectional waves, but it is also observed in counterpropagating waves of equal amplitude in an annulus. The bursting exhibited by each wave is independent of the bursting of the other wave, indicating that the cross coupling between the oppositely propagating components is negligible. The mixtures in the studies had a low weight composition of ethanol (close to 0.40%), and a separation ratio $\psi \gtrsim -0.06$. Dispersive chaos was not observed in a $\psi = -0.069$ mixture[37, 73].

The authors of the one-dimensional “dispersive chaos” studies were able to measure the linear coefficients of the CGLE, as well as the nonlinear frequency renormalization coefficient, c_2 (see Eqn 1.6). They found c_2 to be large, and attributed the irregular growth and collapse of localized convecting regions to strong nonlinear dispersion. Solutions of the CGLE with large c_2 , but no nonlinear cross coupling, show a qualitatively similar erratic bursting behavior[76]. In the simulations, strong dispersion in the absence of the saturating nonlinear cross coupling causes the peak of the envelope of the localized region to grow sharply while its amplitude in the region of strong spatial gradients is damped. As the result, the localized region of convection sharpens and contracts catastrophically. However, this model does not take into account the effect shown to be important to the stability of localized convecting regions, namely the interaction of convection with the concentration field. Inclusion of the concentration field in the model might change the

picture of the chaotic behavior observed in the experiments. My studies of similarly erratic structures in a cylindrical convection cell with low alcohol concentration mixture, suggests that the concentration field dynamics may be an alternative mechanism for spatio-temporal complexity.

Chapter 2

Experimental Set-up

The convection cell containing the fluid sits inside a stainless steel can, as shown in Fig. 2.1. It is thermally insulated from the environment by means of a circulating temperature-controlled water bath and two separate layers of foam insulation. The convection cell itself consists of two plates separated by an annular Delrin spacer sealed to both plates by O-rings. A second temperature controller regulates the bottom plate temperature. The apparatus is optically open from above to enable shadowgraph observation of convection patterns. A detailed overview of the convection apparatus can also be found in deBruyn *et al.*[77].

2.1 Cell Design

One of the most important goals of experiments that are performed close to the onset of convection is to reduce spatial and temporal non-uniformities in the control parameter, i. e. the Rayleigh number $R = \alpha g \Delta T d^3 / \kappa \nu$. A variation in Ra puts some regions of the cell closer to the threshold of convection than others, making detailed comparison with theory difficult. Nonuniformities in Ra are caused by spatial temperature and cell height variations. Since the critical Rayleigh number is proportional to the third